INT. J. REMOTE SENSING, 1994, VOL. 15, NO. 18, 3799–3822

# Image-analysis and cartography of sand hill massifs on high resolution images: application to the Great Western Erg (NW of Algerian Sahara)

Y. CALLOT

Université François Rabelais, URBAMA, Département de Géographie, B.P. 2221, 37021 Tours Cedex, France

C. MERING

Unité de Télédétection, L.I.A., ORSTOM, 72 Route d'Aulnay, 93143 Bondy Cedex, France

and A. SIMONIN

IMAGEO-CNRS, 191 rue Saint Jacques, 75005 Paris, France



*(Received 3 May 1993)*

**Abstract.** The northeastern part of the Great Western Erg (Algerian Sahara) is an area with a continuous cover of coarse sands organized in alignments of large domes separated by corridors where deflation prevails. The domes are covered by small sharp dunes of fine sand (*aklés*). The homogeneity of the substratum does not favour a spectral approach. The cartography of the domes and deflation areas is performed by using the methods of Mathematical Morphology. Panchromatic SPOT images are preferred, because the 10 m pixel resolution is the only unclassified satellite image data that enables differentiation of the landforms. The initial image is processed with grey tone filters in order to homogenize the *aklé* areas. It is next thresholded and the contours of the resulting sets are then regularized. The validation is obtained by comparison with aerial photo-interpretation. At a smaller scale, the orientations of the domes are measured on images from their medial axes.

## 1. Introduction

The geomorphological study of deserts is often limited because of the absence of a large-scale maps and because of the difficulty of conducting field work. Therefore, an analytical approach with airborne or satellite images is the only practical one.

Classical photo-interpretation has been used over a long time to study sand-hill shapes (Clos-Arceduc 1969, Mainguet and Callot 1978). Its major drawback is that it is relatively unquantifiable and requires hand mapping of the shapes. In order to avoid the manual step of photo-interpretation, it is necessary to do the mapping through remote sensing of a series of geomorphological objects in dune environments. Whereas previous work (Mering and Jacqueminet 1987) had used the differences between the vegetation cover of dunes and that of interdune corridors, the absence of vegetation in the area under study led us to design a new approach.

## 2. Presentation of the area

The region selected for the study is the northeastern part of the Great Western Erg, in the Algerian Sahara, about 31°45′ N and 2°40′ E (figure 1), on which two



0143–1161/94 $10.00 

Panchromatic SPOT images (KJ 52/286 and 52/287, 23 December 1989) and a Landsat-TM image (195/038, 25 December 1988) are used. The region is characterized by a well-contrasted dune morphology (Callot 1987, 1991) where four types of dune shapes may be distinguished (figures 2 and 3 (*a*)):

1. Large dune shapes (A in figure 3 (*a*)) forming aligned and often elongated domes of coarse sand, which constitute the main mass of the Erg.
2. *Seifs* (=sabre in Arabic), small dune shapes of fine sand characterized by a sharp and generally curved edge. *Seifs* are organized in *aklé* (B in figure 3 (*a*)), jointed groups of *seifs* of a reticulated aspect. When the accumulation of sand is too abundant on the summits of the domes, *seifs* enlarge and become organized in *ghourds* (star dunes). Most of the time, the *aklé* are superposed on the large dune shapes.
3. *Feidjs*, interdune corridors (C in figure 3 (*a*)) with a thick (several dozen metres) and continuous cover of coarse sand, which correspond to deflation areas.
4. Cauldrons (D in figure 3 (*a*)), closed depressions excavated in the areas of maximum deflation in the sand cover of *feidjs*.

The different spatial scales of these phenomena allow one to reduce the morphology of the Erg into two types of shapes: the set of domes covered with *aklé* on the one hand, and the set of *feidjs* pierced by cauldrons on the other. This duality of shapes is the result of the remarkable stability of the areas of eolian action in the region: the domes correspond to areas of eolian accumulation whose situation has remained unchanged since at least the upper Pleistocene (Callot 1991).

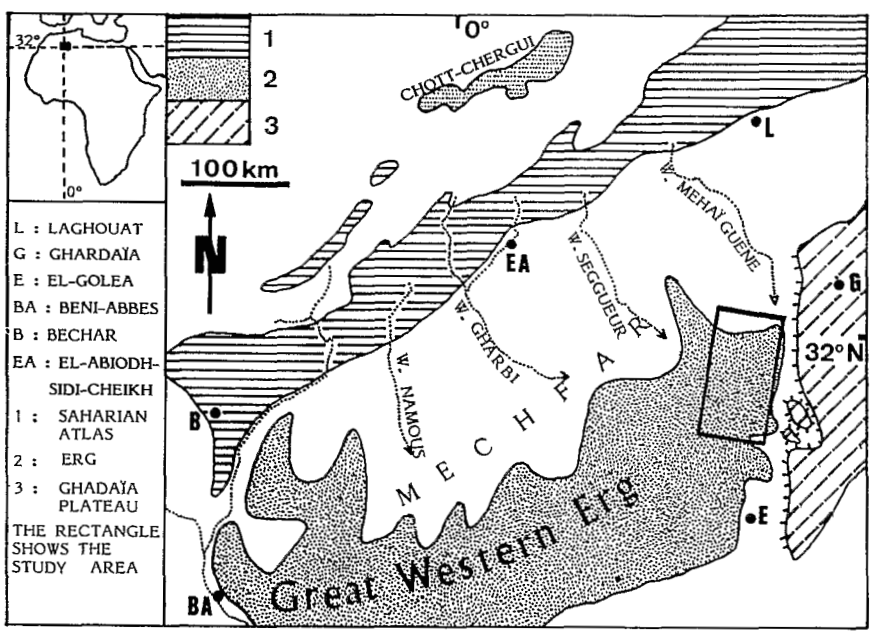


Figure 1. Index map.

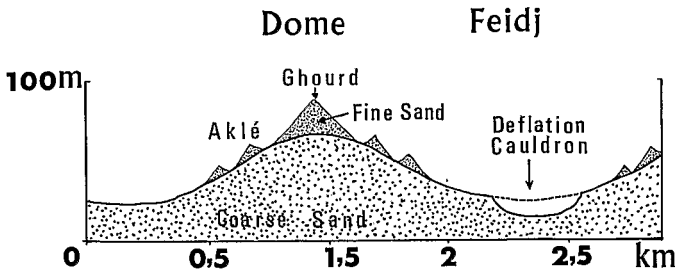


Figure 2. Cross-section of the sand hill shapes NE of the Great Western Erg.

## 3. Cartography by spectral analysis

The first cartographic approach was performed by analysing the spectral response of different forms. However, there exists a remarkable correlation between the 1, 2, 3, 4, 5 and 7 channels of the image named TM.ERG centred on the Erg (table 1). The sixth channel was not selected because of its particular radiometric characteristics and of the resolution power that was lower than that of the other bands. All the types of forms are made up exclusively of sand, which constitutes the homogeneous substratum; this accounts for the marked correlation. The radiometry then mainly expresses the variations in lighting due to the relief on a same surface state (Escadafal 1981).

Using a widely-known technique to perform the automatic segmentation of a scene for cartographic purposes, we have performed several clustering steps by the method of dynamic clusters (Diday 1971) on channels 1, 3, 5, 7 and on the first component of a Karunhene-Loeve Analysis of the 1, 2, 3, 4, 5, 7 channels of the TM.ERG image. The mean spectral responses of the classes thus created are well correlated in all channels: the arrangement of the mean values corresponding to each class for a given channel is identical in all channels. The correlation holds for classifications with 7, 9, 11, 13 and 15 classes (figure 4). In such a case, the result of an automatic multispectral classification can be considered an optimum compression of multi-spectral data (figure 5).

However, though it reduces the number of grey levels to analyse, the classification proves to be insufficient to identify the forms. If we consider a geomorphological object such as a dome, the opposition between its lighted slope and its shaded slope will be clear and will appear in distinct classes. But the heterogeneity of each slope, due to topographical irregularities, is such that it is not even possible to merge the two classes to reconstruct the shape of the dome, because the classes do not contain the totality of the domes when they include other objects. For example, the spectral response of the cauldron slopes which face the Sun is strictly identical to that of the sunny slopes of the domes, and therefore cannot be distinguished on the classified image (see figure 5). The lack of correspondence between the radiometrically homogeneous units and the forms does not allow one to establish a cartographic representation of the geomorphology of the dune massif based only on a multispectral classification.

## 4. Cartography by morphological analysis

### 4.1. *Photo-interpretation and cartography*

The homogeneity of the substratum gives a prominent role to the reflection angle of the radiance in the radiometric response of the images, whichever sensor is used.

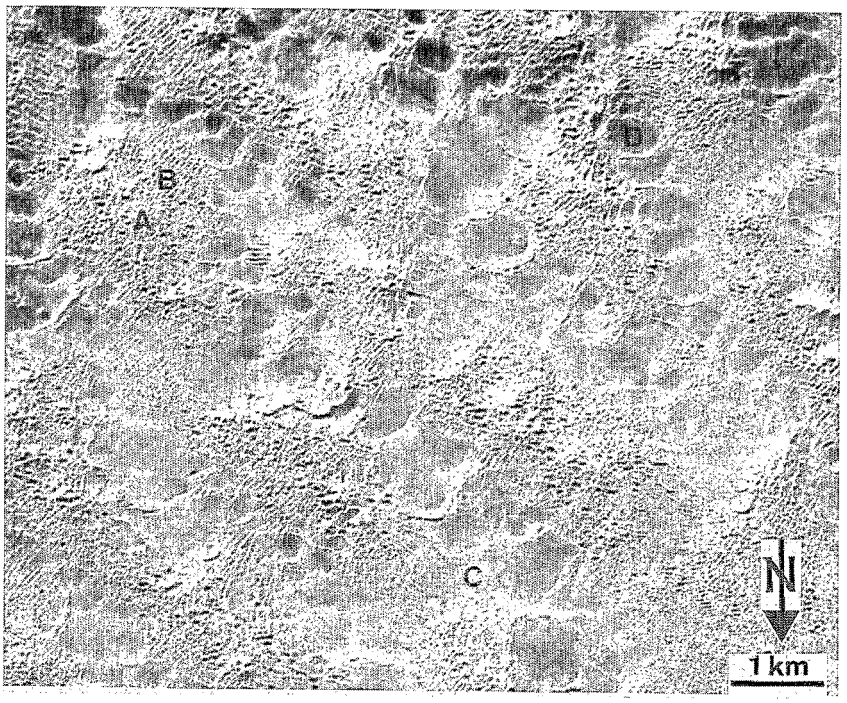


(*a*)

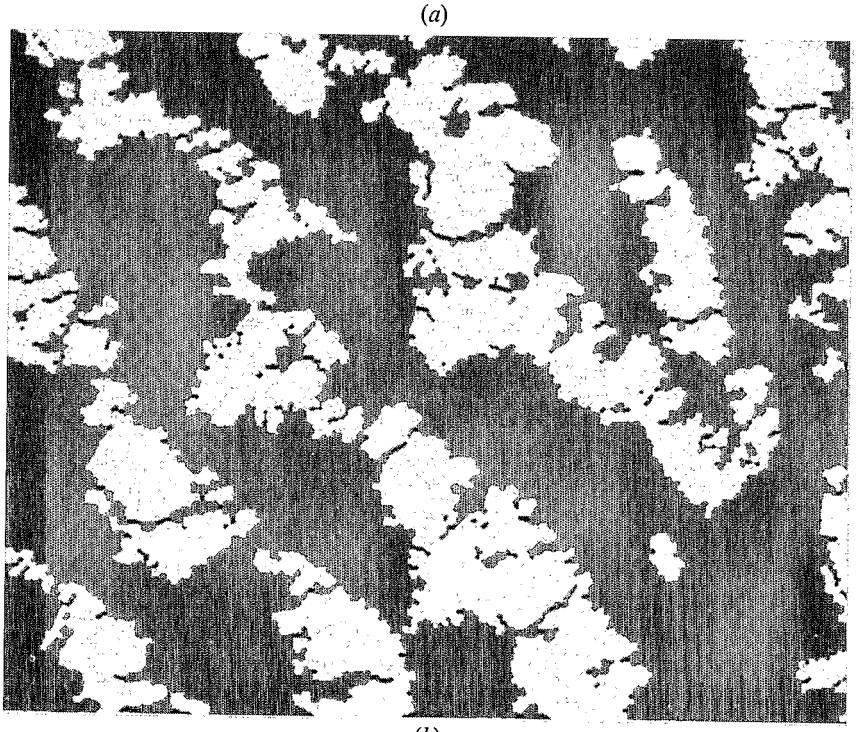

(*b*)

Figure 3. Comparison between a panchromatic SPOT image and its mapping by Mathematical Morphology. (*a*) ERG 1 extracted from the panchro SPOT image 52/27, 23 December 1989 and examples of existing types of forms. (*b*) Automated cartography of the same area.

Table 1. Correlation coefficients between the 1, 2, 3, 4, 5, 7 channels of TM.ERG.

| | Channel 1 | Channel 2 | Channel 3 | Channel 4 | Channel 5 | Channel 7 |
|---|---|---|---|---|---|---|
| Channel 1 | 1·00 | 0·89 | 0·84 | 0·83 | 0·75 | 0·69 |
| Channel 2 | 0·89 | 1·00 | 0·97 | 0·96 | 0·85 | 0·85 |
| Channel 3 | 0·84 | 0·97 | 1·00 | 0·99 | 0·89 | 0·88 |
| Channel 4 | 0·83 | 0·96 | 0·99 | 1·00 | 0·90 | 0·88 |
| Channel 5 | 0·75 | 0·85 | 0·89 | 0·90 | 1·00 | 0·96 |
| Channel 7 | 0·69 | 0·85 | 0·88 | 0·88 | 0·96 | 1·00 |

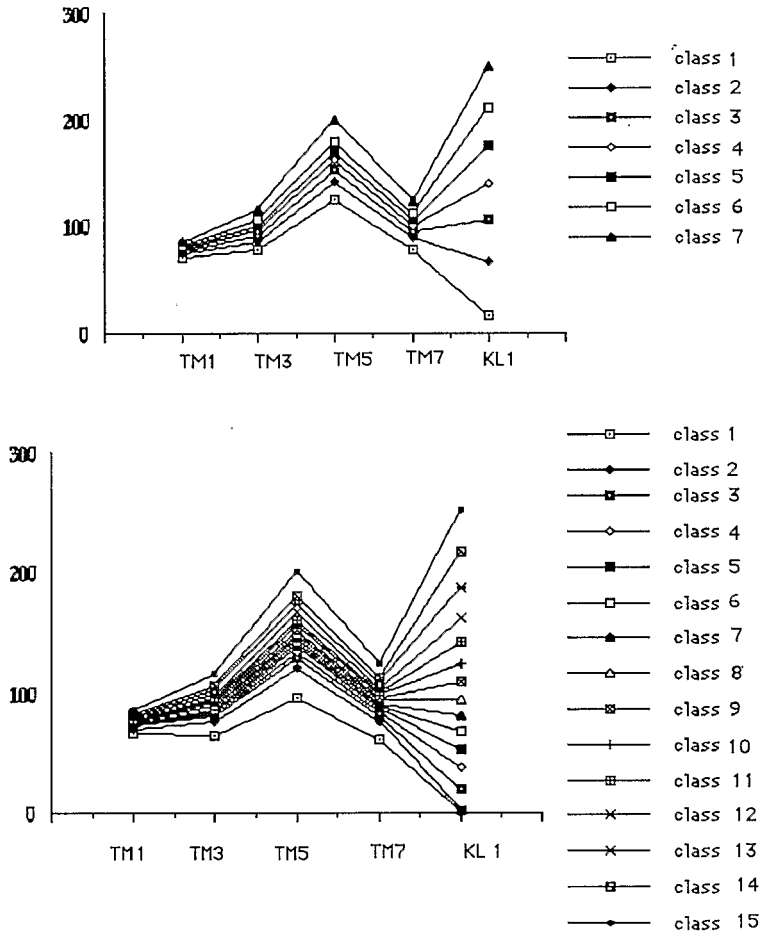


Figure 4. Coordinates of the mean values of four TM channels and the first Karunhene-Loeve component ($KL_1$) within each of the class resulting from both 7 and 15 classes Dynamic Clustering of TM.ERG.

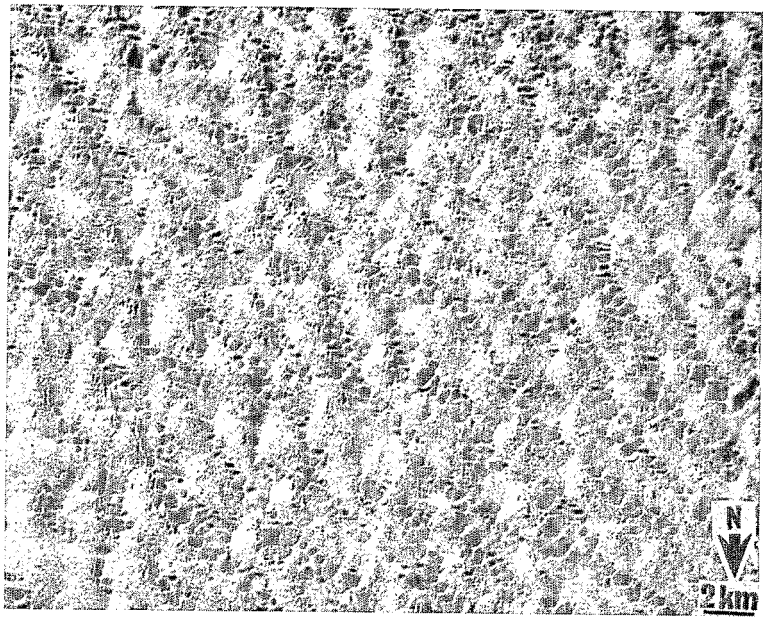


(*a*)

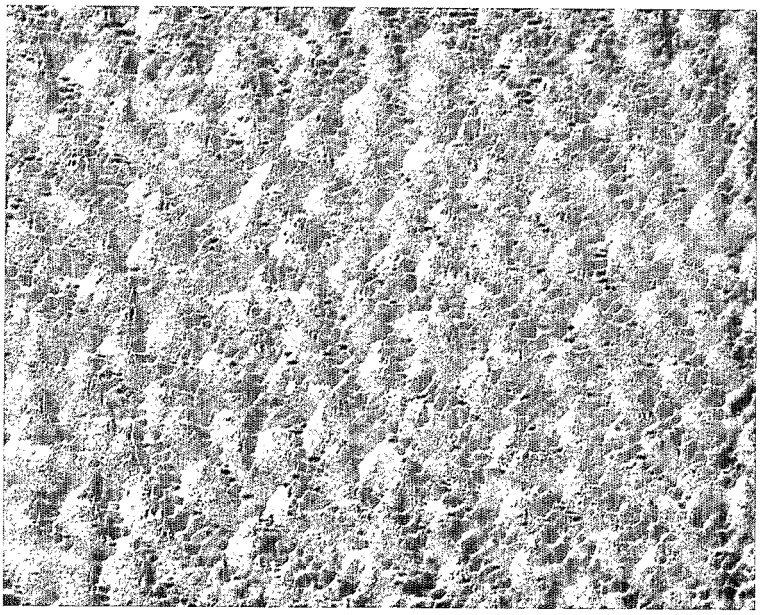

(*b*)

Figure 5. TM.ERG: comparison of a 15 classes-classified image with the first Karunhene-Loeve component image. The channels are so closely correlated that the classification (figure 5 (*a*)) corresponds to a data compression and is not differentiable to the naked eye from the Karunhene-Loeve component of the 1, 2, 3, 4, 5, 7 channels (figure 5 (*b*)).

As the geometry of the forms rules this reflection, the study necessarily goes through the analysis of the forms. Classically, in such cases, photo-interpretation is used in order to identify and extract the desired forms. Photo-interpretation is based on the visual perception of objects from an analog document provided by a vertical (plan) view of the features. As with any visual analysis, there is an effort to structure the image. As numerous studies in the field of cognitive psychology have shown and more particularly those which refer to the Gestalt theory (Köhler 1964), this structuring depends both on the observed object and on the observer who structures the image according to his knowledge and purposes.

In the process of photo-interpretation, structuring is the result of a visual operation and of an interpretation which is transcribed manually in the form of a graphic, such as a map. In numerical image analysis, the structuring can be understood as a gradual transformation of the grey tones. To be able to speak of object extraction, the result of the transformation must be in the form of a binary image. The entities of such an image should correspond to the entities outlined by the photo-interpreter.

This transformation proceeds in simplifying both the texture and the contours. When the texture is simplified, the details which are considered non-significant are eliminated in favour of an homogeneous grey level. The image of the pixels is smoothed into areas of homogeneous grey levels. *Thresholding* allows one to extract a category of objects in the form of a binary image whose contours can be simplified again.

There exist today numerous numerical methods allowing one to perform the simplifying and extracting functions from grey-tone images. They include segmentation (Rosenfeld 1976), smoothing and thresholding methods (Pratt 1978). However, the methods of Mathematical Morphology (Serra 1982) seem more suitable to our study, as they enable the progressive structuring of the images according to the morphological criteria considered relevant by the operator. Our objective is to delimit shape entities that are thematically significant from a grey-tone image. This approach is a type of 'computer-aided photo-interpretation'.

### 4.2. *The principles of morphological transformations. Reminder of the usual methods*

#### 4.2.1. *Morphological transformations on binary images*

Morphological transformations are generally required at the second step of satellite image processing: the numerical image that is analysed is a *binary* image resulting, for example, from the *thresholding* of a grey level image or from a previous classification using several grey-level images as a multi-spectral classification. The set thus defined on the image either corresponds to one threshold value or to one class. Transformations on such a set modify the original structure in order to simplify its shape, particularly by smoothing its contours. The result of such transformations depends on the geometric properties (convexity, anisotropy) of the elementary shape to which the original set is compared.

The set of points of the image whose value is 1 is denoted $X$. In [MM]†, the definition of a *set* is based on the Set Theory. The morphological analysis of the set $X$ of the Euclidian space $R^2$ is obtained by means of *the hit or miss transformation* $\psi$.

†In order to avoid the possible confusion between identical terms in geomorphology and Mathematical Morphology, we have chosen the following terminology: Morphology is always used within the framework of Mathematical Morphology (abreviated MM in the text); the specific terms of MM appear in italics.

$$\begin{aligned} R^2 &\longrightarrow R^2 \\ X &\longrightarrow \psi(X) \end{aligned} \tag{1}$$

These transformations use a *structuring element* of simple geometry such as a disk, a segment, or a hexagon. The *structuring element* $B$ is moved so that its centre $x$ occupies all positions in the Euclidean space. For each position, one verifies if $B$ and $X$ satisfy a certain type of set relation. This relation is expressed in terms of *union*, *intersection* or *inclusion*. The result of such verification can be either positive or negative; this is why such transformations are called *hit or miss transformations* [HMT]. For example, to perform an *erosion*, one verifies, for each point $x$ of the space, if $B$ centred in $x$, is included in $X$. The set of those points $x$ of the space for which the relation is satisfied forms a new set $\psi(X)$ (Coster and Chermant 1989). The *eroded* set $X$, denoted $E^B X$ has an area smaller than $X$, but keeps the same structure (see figures 6 (*b*) and (*c*)). It is said to be anti-extensive. (A transformation $Y$ is called anti-extensive when $Y(X)$ is included in $X$). Similarly, to perform a *dilation*, one verifies, when $B$ is centred in $x$, if the intersection between $B$ and $X$ is not empty. The *dilated* set $X$ (see figures 6 (*d*) and (*e*)), denoted $D^B X$ has an area larger than $X$, but keeps the same structure. It is said to be extensive. (A transformation $Y$ is called extensive when $X$ is included in $Y(X)$). In both cases, contours of the resulting set $\psi(X)$ are more regular than those of set $X$; *Erosion* has eliminated small disconnected entities whereas *dilation* has connected them to the nearest big ones, and filled the smallest holes. Both transformations may be iterated an infinity of times: at the last iteration of the *erosion*, no pixel remains on the image whereas the last step of the *dilation* fills up the whole image.

From *erosion* and *dilation*, two other *hit or miss* transformations are defined, the *opening* $X_B$ and the *closing* $X^B$ as follows:

$$\begin{aligned} X_B &= D^B(E\check{B}X) \\ X^B &= E^B(D\check{B}X) \end{aligned} \tag{2}$$

where:

$\check{B}$ is the transposed element of $B$ with respect to its origin. (The element $\check{B}$ that is identical with $B$ if $B$ has a centre of symmetry which is taken for its origin).

Both of these transformations are more acute than the previous ones. Like *erosion*, *opening* is an anti-extensive transformation, (it may be proved that $X_B$ is included in $X$) and like *dilation*, *closing* is an extensive transformation. (It may be proved that $X$ is included in $X^B$). But at the opposite of the first transformations, the last ones are both *idempotent* (a transformation $Y$ is called idempotent when $Y(Y(X)=Y(X))$. The opened set $X_B$ is more regular, less rich in details, and less expanded than the initial set $X$. The *opening* has smoothed the contours of the connected components, by cutting the narrow ithmuses, suppressing the small islands and the narrow capes (see figures 6 (*f*) and (*g*)). *Closing* is an extensive transformation, (it may be proved that $X$ is included in $X^B$). The *closed* set $X^B$ is more regular and less rich in details than the initial set while it is more expanded. The *closing* also smoothes the contours by filling in the narrow channels, eliminating the small holes and the narrow gulfs (see figures 6 (*h*) and (*i*)).

The last two transformations allow one to structure the image while controlling the modification of the contours of the initial set. However, in certain cases, one merely needs to clean up the set, that is to eliminate the small connected components while preserving all the contours of the largest components, which is not achieved by an *opening*. We can then use a procedure called *reconstruction* which proceeds as follows: once the small components of the initial set $X$ are eliminated by an *erosion* with a convex *structuring element* $B(n)$ of an appropriate size $n$, (i.e., elimination of the largest of the small components), the remaining set is called the *marking set*. At the first step of the algorithm, the *marking set* is dilated by means of $B$. Next the set intersection between $D^B Y$ and $X$ is computed. The resulting set is once more dilated by $B$ and the intersection between the dilated set and $X$ is computed. This operation (*dilation* by $B$ and *intersection* with the original set $X$) is iterated until there is no

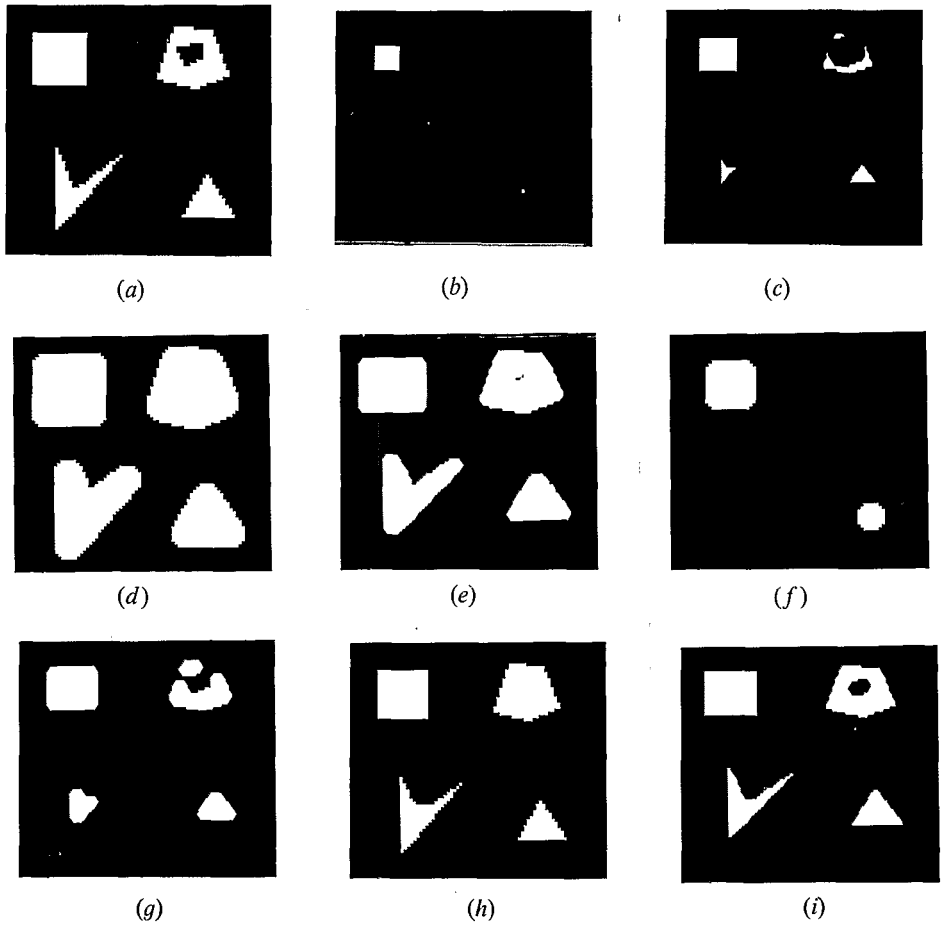


Figure 6. Examples of basic Morphological Transformations on square and hexagonal grids. (*a*) Original sets. (*b*) Erosion of size 2 by an octagon on square grid. (*c*) Erosion of size 2 by an hexagon on hexagonal grid. (*d*) Dilation of size 2 by an octagon on square grid. (*e*) Dilation of size 2 by an hexagon on hexagonal grid. (*f*) Opening of size 2 by an octagon on square grid. (*g*) Opening of size 2 by an hexagon on hexagonal grid. (*h*) Closing of size 2 by an octagon on square grid. (*i*) Closing of size 2 by an hexagon on hexagonal grid.

more modification on the image, (it may be proved that this procedure converges). The reconstruction algorithm is as shown in figure 7.

As we shall see, this procedure is used also to fill the holes of a given size which may exist within the connected entities of a set $X$. To achieve this, it suffices to apply the procedure to the complementary set $X^C$.

4.2.2. *Structuring elements on square and hexagonal grids*

For practical morphological transformations on numerical images, the definition of the structuring elements is connected with the mode of digitalization: from the hexagonal grid, the hexagon is the simplest convex structuring element able to be constructed (figure 8 (*a*)), while from the square grid, the square or the octagon can be chosen as convex structuring elements (figure 8 (*b*)).

According to the digital grid and the structuring convex element, the result of a given *hit or miss* transformation may be perceptibly different, as one can see on figure 6. As remotely-sensed images are originally organized according a square grid, we used this grid for the processing of the SPOT images. The images have been recomputed according to an hexagonal grid only for the detailed studies (figure 10) and for the estimation of the dome alignments (see § 6).

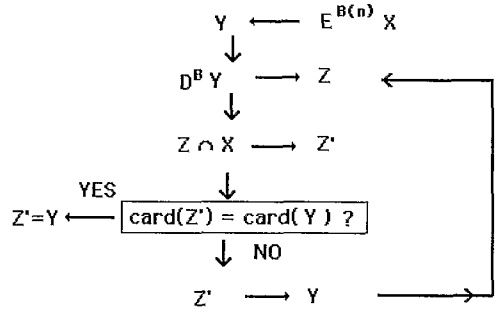


Figure 7. Reconstruction algorithm.

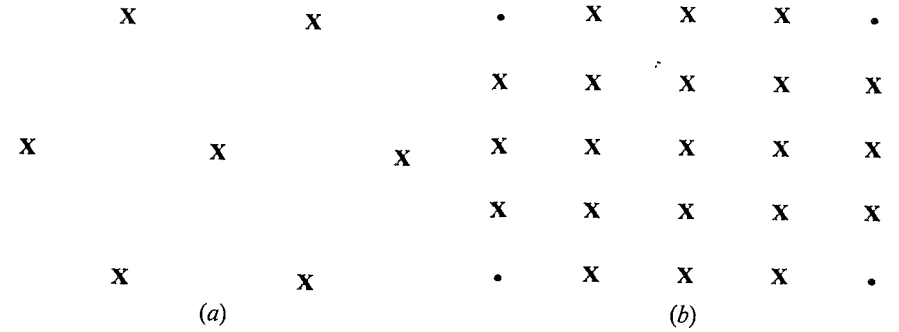


Figure 8. Hexagonal (*a*) and octagonal (*b*) structuring elements of size one designed respectively from the hexagonal and square grid.

4.2.3. *Transformations on digital images*

The transformations presented so far are defined in $R^2$ and not in $Z^2$. Indeed, the digital grid of the images is not considered in the definition of the transformations mentioned above. However, it is sometimes necessary to resort to a digital representation of the image, for instance, when we want to define *homotopic* transformations from digital images, that is, transformations that have the property of preserving the connectivity of the components as well as the number of holes in each of them. Whereas the transformations defined above are not *homotopic*, it is legitimate to expect from the *skeleton* of a set that it possesses such a property. However, the definition of the *skeleton by opening* defined in $R^2$ (Lantuejoul 1980) transposed to $Z^2$ is not *homotopic*. It is then necessary to find transformations suitable to the representation of an image in $Z^2$, that is, based on a raster of points. Then, at each point, transformations are defined according to a given configuration, denoted $V$, of the points on the raster. This neighbourhood configuration $V$ can be considered a structuring element which allows to define HMT in $Z^2$. The neighbourhood configuration $V$ may be defined by three values: 0, 1 and for example a symbolic value such as $x$. The first two values define both the configuration to be tested on the digital image. The third value indicates that the corresponding pixel of the neighbourhood on the image has not to be tested. Let $X$ be a set to be transformed by $V$. Its HMT is written:

$$X \otimes V = \begin{cases} 1 \text{ if } V_x \in V \\ 0 \text{ if } V_x \notin V \end{cases} \tag{3}$$

The HMT operates as follows: when the neighbourhood configuration of the values 0 and 1 on the digital binary image is the same than the corresponding ones on $V$, the central pixel is put to value 1. If not it is put to value 0.

The *thinning* is defined from a HMT using a configuration $V$ as follows:

$$X \bigcirc V = X/(X \otimes V) \tag{4}$$

The *thinning* operates as follows: when the neighbourhood configuration of the values on the digital binary image is the same than the corresponding ones on $V$, the central pixel is put to value 0. If not, the original value remains. The *thinning*, as its name indicates, allows to reduce the surface of a digital set. The choice of a convenient neighbourhood $V$ allows to perform a *thinning* which is homotopic. Lantuejoul (1980) proposed a configuration that allows to obtain a *homotopic skeleton* with a hexagonal raster. This neighbourhood configuration, denoted $L_6$, is the following:

$$\begin{array}{ccccc} & 0 & & x & \\ 0 & & 1 & & 1 \\ & x & & 1 & \end{array} \tag{5}$$

where symbol $x$ means that the value of this peculiar element of the neighbourhood configuration is not to be taken into consideration for the HMT operation.

If successive *thinnings* are performed by 60° rotations of this neighbourhood until convergence of the procedure, a medial form is obtained with a width of one pixel which preserves the connectivities and the holes of the initial structure and which is called a *homotopic skeleton* (Lantuejoul and Maisonneuve 1984). As we

shall see further (see § 6), this *skeleton* allows to study the orientations of the resulting sets.

4.2.4. *Morphological transformations on grey-level images*

Mathematical Morphology may be required to achieve the first step of the grey-tone image structuration, that is the smoothing of the grey-tone texture. Another use of [*M.M.*] on grey-tone images is the morphological filtering that is the enhancement of some dark or light structures of given morphology.

Definitions of morphological transformations on sets are generalized to transformations on grey-tone images by considering that a grey-level image is defined by a function $f(x)$ in $R^2$, where $f(x)$ represents the numerical value, that is the level of point $x$ (Serra 1982) where each point is associated a *structuring element B*. In the domain defined by $B$ around $x$, $f(x)$ has a superior value and an inferior value.

To obtain the function eroded by the *structuring element B*, it suffices to assign to each point of the domain the inferior value of $f(x)$ in this domain, which is written:

$$E^B f(x) = inf\,\{f(u) : u \in B_x\} \tag{6}$$

Similarly, to obtain the function dilated by the *structuring element B*, it suffices to assign to each point of the domain $B_x$ the superior value of $f(x)$ in this domain, which is written:

$$D^B f(x) = sup\,\{f(u) : u \in B_x\} \tag{7}$$

To simplify the illustration, consider the grey-tone function $f(x)$ of an image defined in $R^1$, where $f(x)$ is positive since $f(x)$ corresponds to a level of lighting. This function may be considered to belong to the space $R^2$ in which every point would be defined by $x$ and $t$. Then we can consider the subgraph $U_f$ of $f(x)$ defined by:

$$U_f = \{x,t : t \leq f(x)\} \tag{8}$$

If the subgraph $U_f$ of $f$ is considered a relief as in figure 9 (*a*), it may be noticed that an *erosion* reduces the peaks and widens the valleys, whereas a *dilation* thickens the peaks and fills the valleys.

The morphological *opening* and *closing* of a function $f$ are defined likewise, by analogy with set transformations.

If we refer to § 4.2.1., we can define the *opening* of a function $f$ by a *structuring element B* as follows:

$$f_B(x) = D^B(E^B f(x)) \tag{9}$$

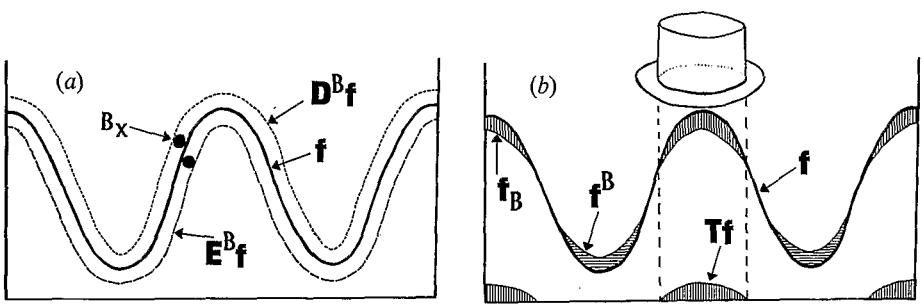


Figure 9. Morphological transformations of a function. (*a*) *Erosion* and *dilation*, (*b*) *Opening*, *Closing* and *Top Hat*.

Similarly, the *closing* $f^B$ of a function $f$ by a *structuring element* $B$ is defined as follows:

$$f^B(x)=E^B(D^Bf(x)) \tag{10}$$

These transformations only modify certain points of a grey level image: an *opening* erodes the sharp peaks and a *closing* fills the narrow valleys of the relief with which the subgraph $U_f$ is identified, as may be seen on figure 9 (*b*).

The properties of these transformations are used to define morphological filters such as *top hats*. These filters allow one to extract only the peaks from a grey level image (the small light elements), or only the valleys (the small dark elements). Thus, by computing the difference between the initial image and its *opening* by a *structuring element nB*, the peaks whose thickness is less than $n$ are extracted (see figure 9 (*b*)). This can be expressed as follows:

$$Tf(x)=f(x)-f_{nB}(x) \tag{11}$$

Similarly, to extract the valleys whose thickness is less than $n$, it suffices to compute the following expression;

$$Tf(x)=f^{nB}(x)-f(x) \tag{12}$$

## 5. Cartography of eolian forms

### 5.1. *Methodology*

Images are composed of sets, the shapes of which are often elongated. The sets have a different texture: the domes covered with *aklé* are contrasted and light; their heterogeneous aspect is due to the light-shade contrasts in the small sharp-edged dunes. The domes are separated by deflation areas of similar shape, homogeneous texture, and of darker tone (figure 3). Because our approach aims at individualizing each of the two sets, we used the great difference in texture between *aklé* areas (corresponding to domes) and deflation areas (corresponding to interdune corridors).

As the definition of the domes requires one to define first the *aklé* which covers them, Panchromatic SPOT images are preferred because their spatial resolution ($10 \times 10$ m) is the only one that enables the detection of the individual *seifs*. The tests performed from the spectral bands corresponding to the visible field of Landsat-TM images do not provide this degree of differentiation: the dimensions of the *seifs* are so small that their lighted sides, whose spectral response is high, never constitute the sole element of one pixel of a ($30 \times 30$ m) Landsat-TM image, which always includes elements in the shade. The result is a marked reduction in the contrast between *aklé* areas and deflation areas, which makes the processing ineffective.

The processing requires two steps. The first one consists in homogenizing the grey tones of the areas to be detected. The *thresholding* of the resulting grey levels enables the first segmentation of the image, which corresponds to a rough delimitation of the sets 'dome/deflation areas'. The second step consists in a more accurate contouring of the sets on the binary image resulting from the *thresholding*. The processing proceeds through *sequences* of *morphological grey-tone transformations* in order to achieve the first step, and through *sequences* of binary transformations to achieve the second one. A *sequence* consists in at least two *morphological transformations*, the purpose of which is to determine a set or a measurement on a set. A simple *sequence*, such as *reconstruction*, may be integrated into a more complex one (see

below). Some *sequences* may be entirely automated. In the present case, it is not so: the grey-tone *thresholding* is the only operation performed by the operator.

The final result of the study is a map of sharp dune and deflation areas. Deflation corresponds to interdune corridors, and we can then obtain a map of the dune structures of the Erg, with the great domes and their *aklé* on the one hand (the domes are generally aligned) and with the interdune corridors and their cauldrons on the other hand.

5.2. *Morphological transformations for extracting deflation areas*

The deflation areas are deduced from the delimitation of the light areas that correspond to sharp dunes, because the deflation areas form a complementary set with respect to the sharp dunes set. This is achieved by smoothing the contrasted textures of *aklé* areas into light areas without modifying the homogeneity of the dark deflation areas, so that the same grey tone is associated with the relevant set.

All the transformations use an octagonal *structuring element* which as far as possible does not favour any particular orientation and which does not require one to change the original square grid of satellite images.

The grey level of the edges of the *seifs* facing the Sun is very high. Their detection is then possible by means of a *top hat* (figure 10 (*b*)) from an *opening* of size 1.

From this processing, we obtain only the *aklé* edges in the form of striped areas, where the remaining dark zones correspond to the shadowy part of the dunes and to the small sandy areas between the *seifs*. As the dark interdune areas are quite narrow, they can be eliminated by covering them with a marker that invades the dune area after a *dilation* of size 2 (figure 10 (*c*)).

The greytones are then sufficiently homogeneous and differentiated to enable the delimitation of the two desired sets, since we have now a binary image. A *thresholding* with an upper limit is selected in order to obtain a binary image which approximately corresponds to the set of deflation areas (which appear in white) which is the complement of the set of dune areas defined by the previous processing. After a screen examination, the *thresholding* has been set to a grey value of 9 which gives surfaces (figure 10 (*d*)) whose area compares with that of the deflation areas defined by direct observation on the original SPOT image.

The resulting set is larger than the areas observed on the ground. A sequence of binary *morphology* has been designed to eliminate the scattering of small isolated entities, since they should not be identified with deflation areas but with small interdune zones in *aklé* areas.

We must first eliminate the isolated sets whose radius is less than 3 pixels by a *reconstruction* (figure 10 (*e*)) from a marker obtained by an *erosion* of size 2 of the previous set. The result of the *reconstruction* solely preserves large connected areas. A *reconstruction* is a much less severe transformation than an *opening*, because it preserves the original contours of the sets, while suppresssing only the small entities which are disconnected from the main sets. The small holes which remain inside large deflation areas are eliminated by a *reconstruction* of the complementary set to which has been applied an *erosion* of size 2. The final image (figure 10 (*f*)) corresponds to the desired set of deflation areas. Figure 3 presents the original scene and the corresponding cartography performed according to the sequence shown in table 2.

5.3. *Validation of automated cartography*

In the cartography of forms based on *Morphological Analysis*, there does not exist any standard validation method that can be used for the method of multi-spectral classification. In the latter case, confusion matrices are produced, which indicate the number of rightly or wrongly classified pixels from small test zones. The small dimension of the zones is legitimate for the classification of surface states. In the case of the cartography of forms, the validation concerns all the forms, and therefore has to consider a part of the image that contains enough forms to be

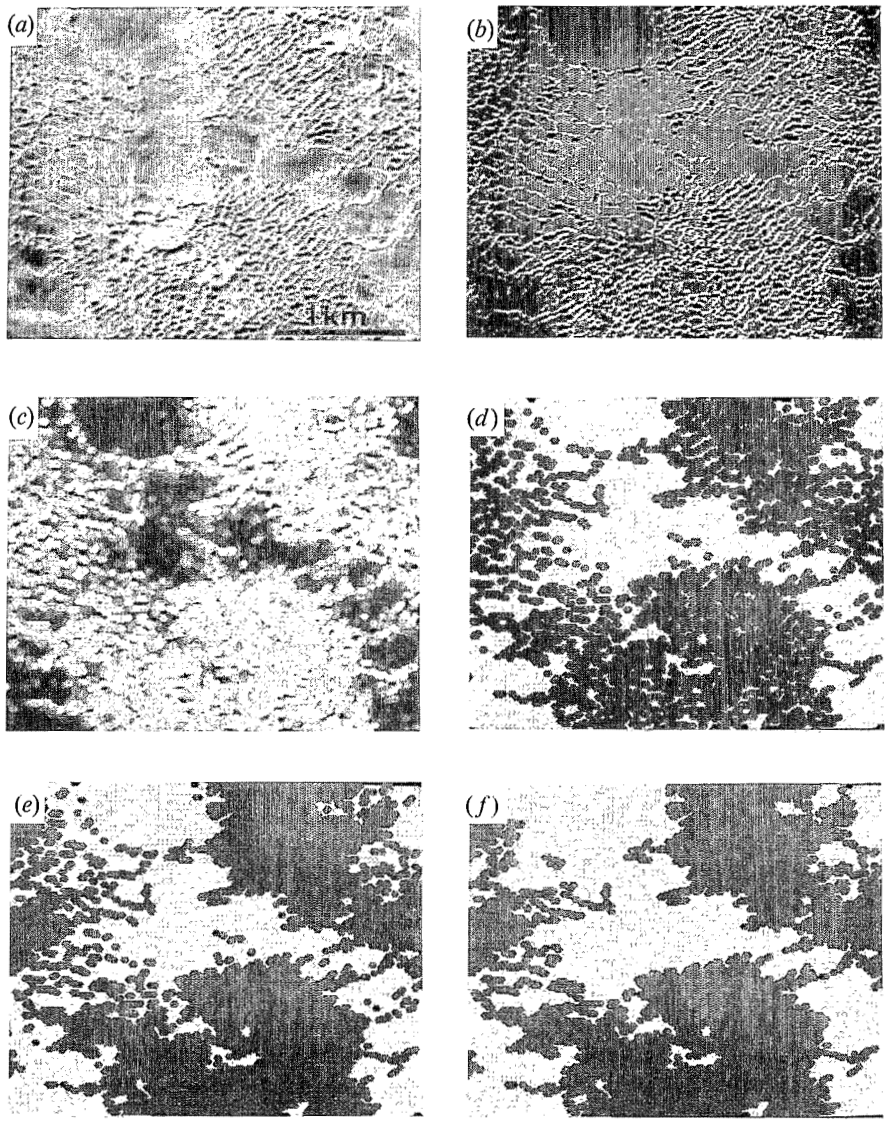


Figure 10. Sequence of transformations for delimiting deflation areas. (*a*) Initial image. (*b*) *Top hat*. (*c*) *Dilation* of size 2. (*d*) *Thresholding*. (*e*) *Reconstruction*. (*f*) Final image after the filling of small holes.

Table 2. Sequence for the cartography of deflation areas.

| | |
|---|---|
| Opening of size 1 | Detection of the: |
| *Top hat* | —*seifs* |
| Dilation of size 2 | —*aklés* |
| Binarization with a threshold at 9 | Determination of |
| Erosion of size 2 | the deflation areas |
| Reconstruction | Filling of the holes |
| Complementation | |
| Erosion of size 2 | |
| Reconstruction | |
| Complementation | |

representative. This is the reason why we use a validation method which compares the map produced by computation with the one produced by photo-interpretation done by a single person. Each type of cartography is associated by a set of the Euclidean space and the validation bears on the measurement of the *symmetrical difference* $Y$ between the two sets $X$ and $X'$, where:

$$Y=(X \cup X')/(X \cap X') \tag{13}$$

Here, the measure of the set $Y$ has to be minimized.

The cartography of the deflation areas was performed manually by the zoning of a Panchromatic SPOT image based on two testing zones of $900 \times 750$ pixels ($9 \times 7{\cdot}5$ km). The first one corresponds to an area of complex structure where *aklés* predominate (ERG 1, figure 11), the second one corresponds to a simpler structure where deflation areas are more expanded (ERG 2, figure 12).

The images of the *symmetrical difference* between photo-interpretation and automated cartography show the great differences between ERG 1 and ERG 2 (table 3). In complex areas (figure 11), the estimated error is superior: the interpreted deflation areas are larger than the computed ones. In simple areas (figure 12), the photo-interpreted zones in deflation areas that have not been taken into account by automated cartography are more similar to the surfaces considered as deflation areas by automated cartography and not by photo-interpretation.

## 6. Orientation of eolian forms

A second sequence has been designed in order to study the orientations of the sandy domes which are organized in more or less triangular directions. The sequence was adjusted in the NE quarter of the Panchromatic SPOT image 52/287 acquired on 23 December 1989. Because the study of the directions does not require one to know the details of the inside structure of the domes, the image is incremented 8 times by direct sampling. A smoothing by the mean value cannot be used because it reduces the contrast between extreme grey-tone values, on which morphological processes are based. Direct sampling eliminates the elongated structures of the *aklés*, which are replaced by the dotted texture corresponding to the juxtaposition of pixels with high and low reflectance sampled on the lighted and shaded sides of the *seifs*.

Next, the image is computed according to a hexagonal grid (figure 13 (*a*)) and is processed with a hexagonal structuring element. This transformation is due to the

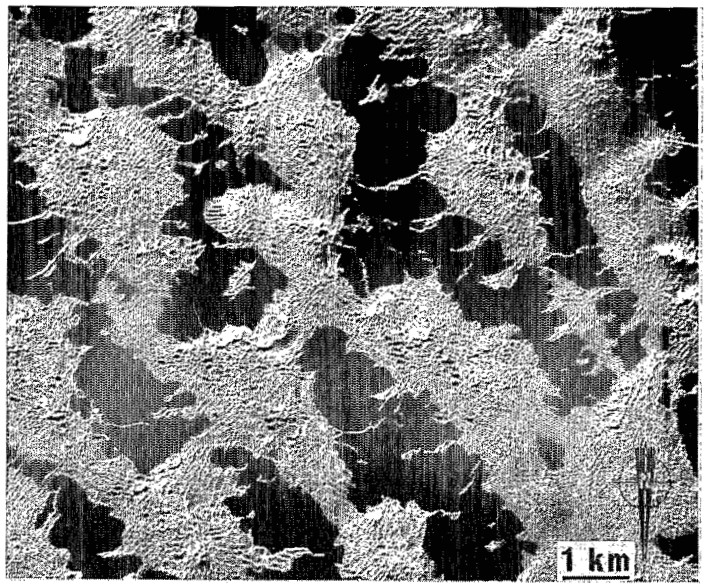


(*b*)

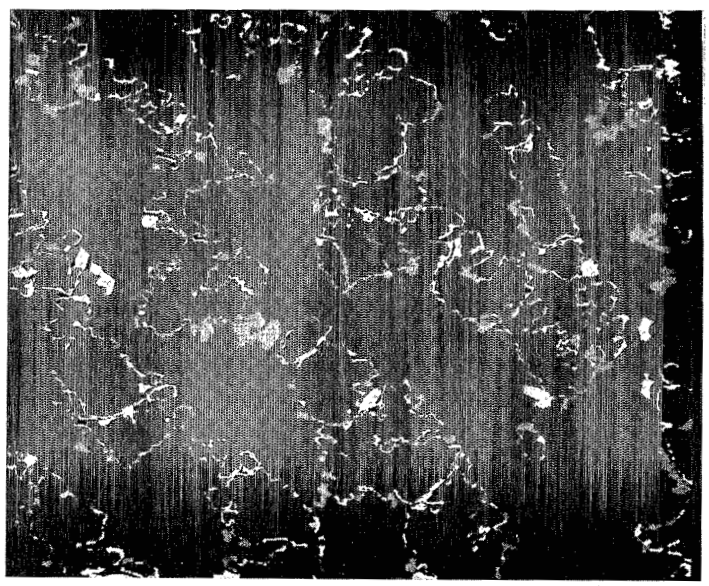

(*b*)

Figure 11. Photo-interpretation of the image ERG1 and *symmetrical difference* between photo-interpretation and automated cartography. (*a*) Photo-interpretation. (*b*) *Symmetrical difference.* The white areas correspond to the surfaces photo-interpreted in deflation areas but not taken into account by automated cartography. The grey areas correspond to the surfaces considered as deflation areas by automated cartography and not by photo-interpretation.

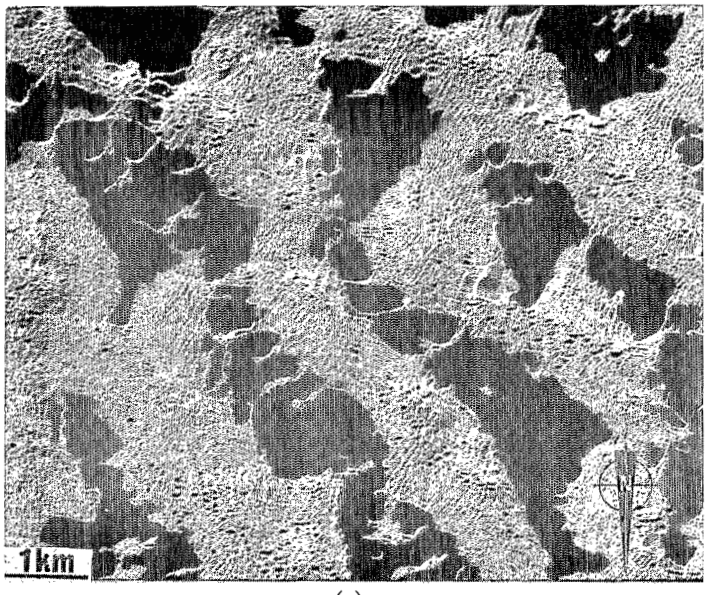


(*a*)

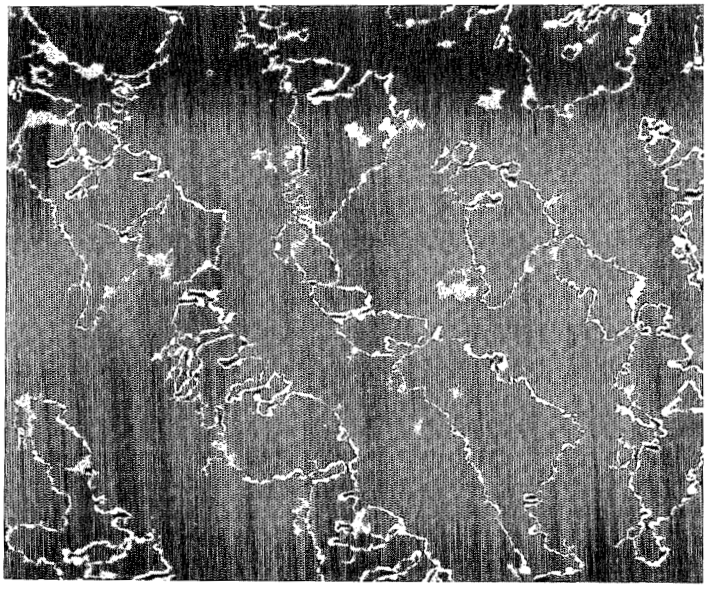

(*b*)

Figure 12. Photo-interpretation of the image ERG2 and *symmetrical difference* between photo-interpretation and automated cartography. (*a*) Photo-interpretation. (*b*) *Symmetrical difference*. (Same legend as figure 11 (*b*)).

necessity of using a structuring element symmetrical with respect to its centre so as to obtain a perfectly isotropic configuration to study the directions.

6.1. *Detection of light areas*

The brightest points are selected by a grey-tone morphological transformations that uses a *top hat* (figure 13 (*b*)) from an *opening* of size 1. The result is too dotted

Table 3. Quantified validation.

| | $Y_1$ (%) | $Y_2$ (%) | Total error (%) |
|---|---|---|---|
| $ERG_1$ | 9 | 2 | 11 |
| $ERG_2$ | 5 | 3 | 8 |

because of the rapid alternation of the low-reflectance pixels of the shadowy areas of the *aklés* and the high reflectance pixels of their lighted sides.

To smooth the effect of the filtering, a *closing* of size 2 is applied (figure 13 (*c*)). The light areas of the image roughly correspond to the set of domes. A binarization with a threshold at 11 produces surfaces whose areas correspond to those of the domes. We use this image as a reference (figure 13 (*d*)).

6.2. *Delimitation of the sets of domes*

A particularity of the binarized image is to contain other sets than the domes:

1. The *seifs* bordering the northern slopes of the large deflation cauldrons form non-connected sets
2. The boundaries of the domes are connected with *seifs* that penetrate the deflation areas; although they are not very significant in terms of area, they introduce divergent secondary directions which may bias the estimation of the major preferential orientations
3. In the centre of the dome areas, some dark zones remain (holes) of small size which correspond to the shadow of the largest *ghourds*.

Three successive types of procedures enable the elimination of each of these sets. The isolated sets of small size are eliminated by a reconstruction using the original binary image as a mask and its erosion of size 2 as a marker.

An *opening* modifies too much the boundaries of the sets of domes to be used for eliminating the connected sets. *Thinnings* by means of a linear neighbourhood (figure 14) are therefore preferred, because they preserve the connectivity of the sets and allow one to control the orientation of the elements to be suppressed. The thinnings are iterated in all directions of the hexagonal grid (0, 60, 120, 180, 240, 300) to eliminate the following configurations in all directions: lines of 3 pixels, angled lines, lines of 2 pixels, triangles and isolated pixels. The result of the thinnings is reconstructed after an erosion of size 2, which suppresses the small isolated sets disconnected from the large entities by this process (figure 13 (*e*)).

The elimination of the shadowy zones in the center of domes cannot be obtained directly, because the resulting image contains 'holes' of different sizes. Large 'holes' are actually deflation areas included in sets of domes. Therefore, as in the case of deflation areas, a reconstruction is applied to the complementary set by means of the marker obtained by an erosion of size 2. A second complementation gives the final image (figure 13 (*f*)).

6.3. *Estimation of the orientations of the domes alignments*

6.3.1. *Estimation methods*

Major orientations are estimated from local orientations in a given neighbourhood of pixels. The reference system is anti-clockwise: 0° corresponds to the east, 90°

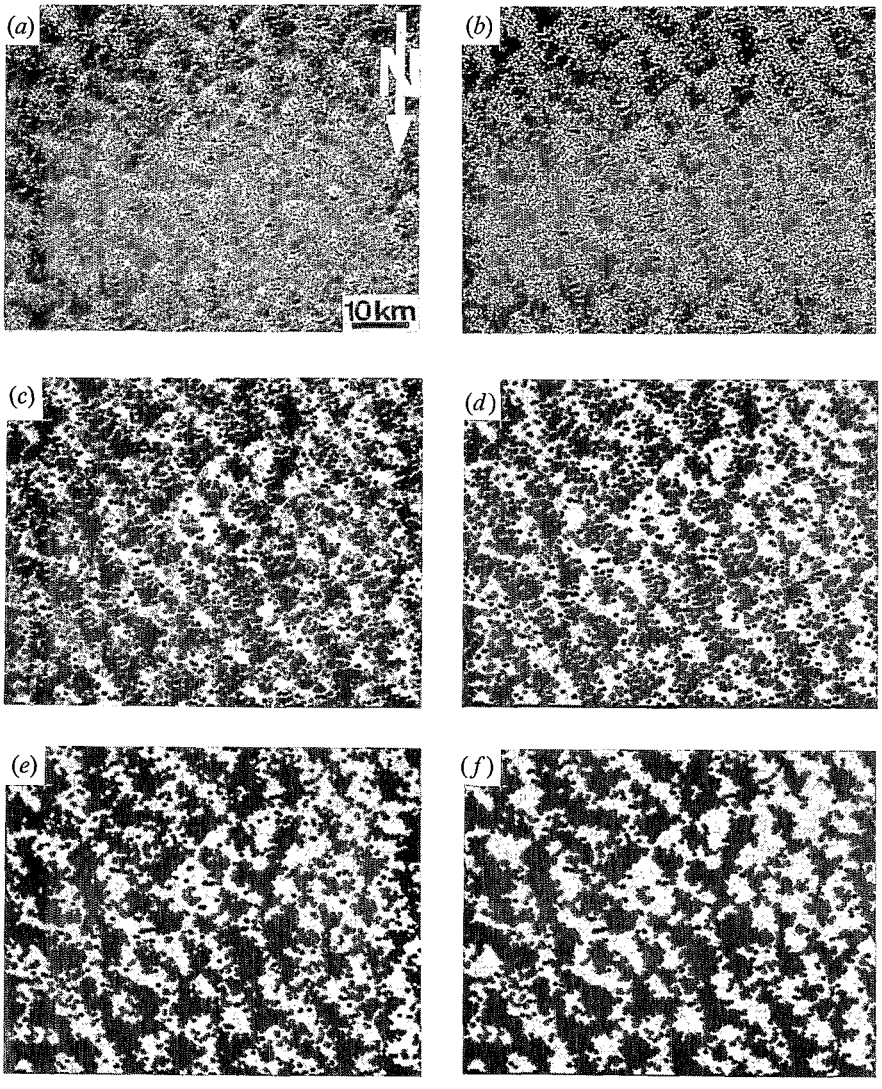


Figure 13. Sequence of transformations for delimiting sandy domes. (*a*) Initial image. (*b*) *Top hat*. (*c*) Closing of size 2. (*d*) Thresholding set to 11. (*e*) Thinnings. (*f*) Final image after the reconstruction of the complementary set.

east to the north, 180° to the west, and 270° to the south. The procedure consists in identifying each of the twelve directions given by the hexagonal grid with a series of neighbourhood configurations. For example, the direction 0° is identified with a series of five configurations (figure 15).

Each direction is incremented according to the configuration found on the image. We finally obtain a *Rose of directions* which characterizes the set under study.

Two approaches are adopted. The first one, by analogy with the approach of photo-interpretation, tries to specify the directions of the contours in the case of objects with a complex geometry which do not present any preferential direction

Table 4. Sequence for the cartography of the areas of domes.

| | |
|---|---|
| Opening of size 1<br>*Top hat* | Detection of the:<br>areas of *seifs* |
| Closing of size 2<br>Binarization with a threshold at 11 | Detection of the<br>domes |
| Erosion of size 2<br>Reconstruction | Elimination of small<br>isolated entities |
| Thinnings<br>Erosion of size 2<br>Reconstruction | Regularization of<br>the contours |
| Complementation<br>Erosion of size 2<br>Reconstruction | Filling of the holes |

(sub-isotropic objects)—the visible directions belong to the alignments of neighbouring or jointed object contours. The contours are delimited by means of a *morphological gradient* that consists in computing the difference between the dilated and the eroded sets. To this result is applied a skeleton in order to reduce the thickness of the contour to one pixel. This is achieved in figure 16 (*a*) by a *homotopic skeleton by thinning* (Lantuejoul and Maisonneuve 1984) (see above).

The second approach uses the concepts and the tools of automated image analysis. The orientation of an object is no longer that of its contour but the orientation of its medial axis. In this case, the *homotopic skeleton by thinning* is applied on the set itself (figure 16 (*b*)) and its *Rose of directions* computed.

6.3.2. *Orientations of the domes*

The comparison between the *Rose of directions* of the contours (figure 17 (*a*)) and that of the medial axes (figure 17 (*b*)) shows that the latter better emphasizes the prevailing directions. The main orientation of the domes, NNW–SSE, is obvious with a value twice as high as the least representative directions, such as WNW–ESE. The other main orientations, E–W and NNE–SSW, are also clearly noticeable. On the other hand, in the *Rose of directions* of the contours, the order of the main

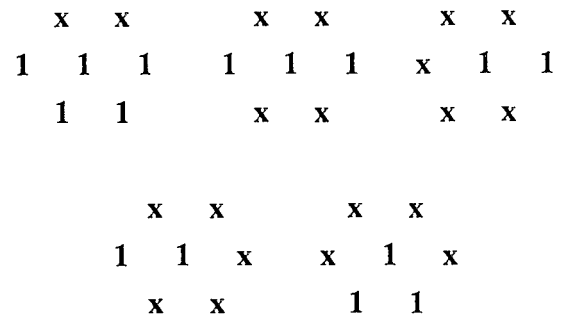

Figure 14. Neighbourhood configurations used for the thinnings.

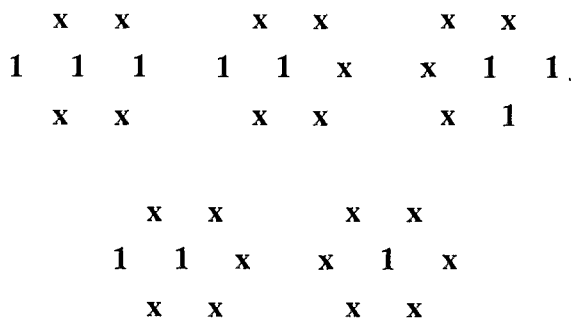


Figure 15. Neighbourhood configuration corresponding to the direction 0°.

directions is preserved, but the values are closer because all intermediate directions of the contours are taken into account. Even if it is possible to compensate for this inconvenience with a modification of the origin (by subtracting 1000 measures from each direction for example), it is preferable to use the *Rose of directions* of the medial axes.

## 7. Conclusion

Mathematical Morphology applied to Panchromatic SPOT images of the Great Western Erg proves to be a suitable tool for studying this kind of environment with a low error rate. The applied method may be generalized to other ergs. Forms with sharp edges and with a marked contrast between the lighted and the shadowy slopes are found in most dune massifs around the world, in which they contrast with the characteristic round shapes of coarse sands or sands fixed by vegetation. The sequence of morphological transformation introduced here allows one to distinguish *aklé* areas, with fine and unstable sands, which are an immediate danger for the environment, from more stable areas that are dangerous at present, but still liable to deteriorate. This study focuses on cartography; however similar approaches may

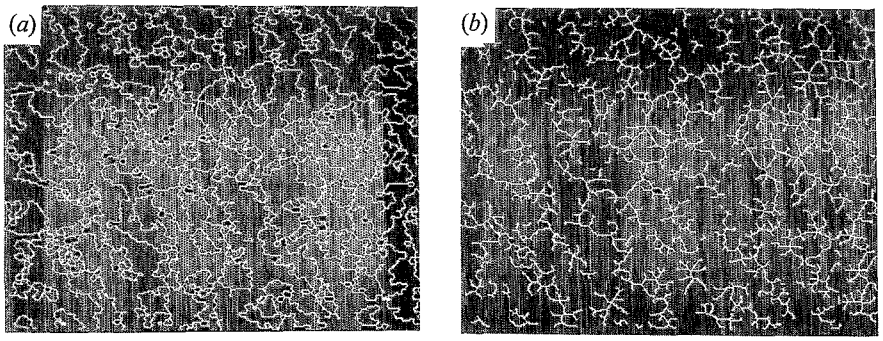


Figure 16. *Homotopic skeletons* of the sandy domes area. (*a*) *Skeleton* of the contours. (*b*) *Skeleton* of the medial axis.

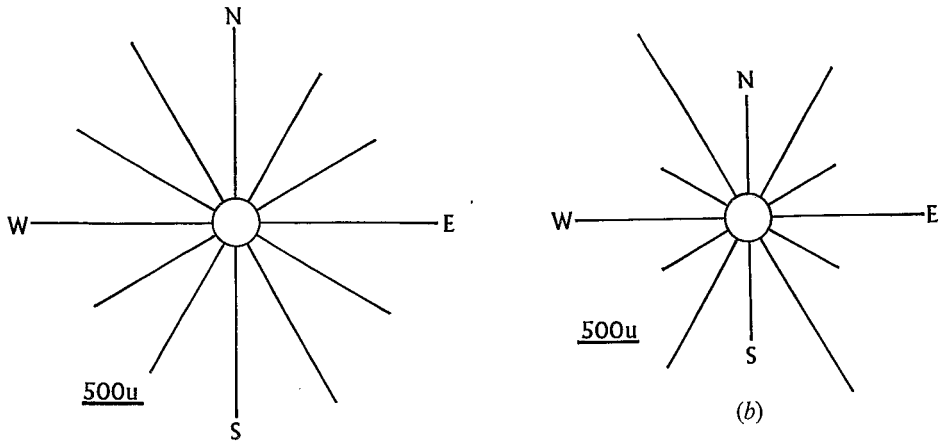


Figure 17. *Roses of directions* of the sandy domes. (*a*) of the contours; (*b*) of the medial axes.

find practical applications in more inhabited areas for development and planning purposes.

**Acknowledgments**

This work has been supported by the P.N.T.S. (Programme National de Télédétection Spatiale). The standard sequence has been elaborated from the extraction of a 300 columns by 256 lines area transposed on a hexagonal grid by the software programme MORPHO (O.R.S.T.O.M.) developed from the original algorithms of MORPHOLOG (Centre de Morphologie Mathématique, E.N.S.M.P., Fontainebleau, France). The sequence has been extrapolated to a quarter of a SPOT scene by using equivalent programs of the software program PLANETES (O.R.S.T.O.M.), that processes entire scenes in square grid. The text was read and edited by Dr M. F. Davie, to whom thanks are extended.

**References**

CALLOT, Y., 1987, Géomorphologie et paléoenvironnements de l'Atlas Saharien au Grand Erg Occidental: dynamique éolienne et paléo-lacs holocènes, (Thesis, Université Pierre et Marie Curie, Paris) *Mémoires des Sciences de la Terre*, 87-21.

CALLOT, Y., 1991, Le Grand Erg Occidental (Algérie). Histoire d'un massif de dunes. *Science et changements planétaires—Sécheresse*, **2**, 26-39.

CLOS-ARCEDUC, A., 1969, *Essai d'explication des formes dunaires sahariennes* (Paris, Institut Géographique National), *Etudes de photo-interprétation*, **4**.

COSTER, M., and CHERMANT, J. L., 1989, *Précis d'analyse d'images* (Paris, C.N.R.S.).

DIDAY, E., 1971, La méthode des Nuées Dynamiques. *Revue de Statistique Appliquée*, **19**, 19-34.

ESCADAFAL, R., 1981, Une méthode nouvelle de description de surface des sols dans les régions arides, *3d Colloque Association Internationale de Science des Sols.: Traitement informatique des données de sols, Paris, 1981*, *Sols*, **4**, 21-27.

KÖHLER, W., 1964, *Psychologie de la forme*, (Paris: Gallimard), pp. 174-175.

LANTUEJOUL, C., 1980, Skeletonization in Quantitative Metallography. In *Issues of Digital Image Processing*, edited by R. M. Haralick and J. C. Simon (Alphen ann den Rijn: Sijthoff and Noordhoff) pp. 107-135.

LANTUEJOUL, C., and MAISONNEUVE F., 1984, Geodesic Methods in Quantitative Image Analysis. *Pattern Recognition*, **17**, 177-187.

MAINGUET, M., and CALLOT, Y., 1978, *L'Erg de Fachi-Bilma (Tchad-Niger). Contribution à la connaissance de la dynamique des ergs et des dunes des zones arides chaudes*, (Paris: C.N.R.S.), Mémoires et Documents, **18**.

MERING, C., and JACQUEMINET, C., 1987, An Approach of Quantitative Description of Sand-hill Shapes in the West African Sahel from Remote Sensing Imagery. *International Congress of Stereology, Caen, 1987* (Ljubljana: *Acta Stereologica*), pp. 951–956.

PRATT, W., 1978, *Digital Image Processing* (New York: Wiley).

ROSENFELD, A., 1976, *Digital Picture Processing* (London: Academic Press).

SERRA, J., 1982, *Image Analysis and Mathematical Morphology* (London: Academic Press).